Hybrid Antimicrobial Enzyme and Silver Nanoparticle Coatings for Medical Instruments

D. Matthew Eby,*,†,‡ Heather R. Luckarift,†,‡ and Glenn R. Johnson*,‡

Microbiology and Applied Biochemistry, Materials and Manufacturing Directorate, Air Force Research Laboratory and Universal Technology Corporation, 139 Barnes Drive, Suite 2, Tyndall AFB, Florida 32403

ABSTRACT We report a method for the synthesis of antimicrobial coatings on medical instruments that combines the bacteriolytic activity of lysozyme and the biocidal properties of silver nanoparticles. Colloidal suspensions of lysozyme and silver nanoparticles were electrophoretically deposited onto the surface of stainless steel surgical blades and needles. Electrodeposited films firmly adhered to stainless steel surfaces even after extensive washing and retained the hydrolytic properties of lysozyme. The antimicrobial efficacy of coatings was tested by using blades and needles in an in vitro lytic assay designed to mimic the normal application of the instruments. Coated blades and needles were used to make incisions and punctures, respectively, into agarose infused with bacterial cells. Cell lysis was seen at the contact sites, demonstrating that antimicrobial activity is transferred into the media, as well as retained on the surface of the blades and needles. Blade coatings also exhibited antimicrobial activity against a range of bacterial species. In particular, coated blades demonstrated potent bactericidal activity, reducing cell viability by at least 3 log within 1.5 h for *Klebsiella pneumoniae*, *Bacillus anthracis* Sterne, and *Bacillus subtilis* and within 3 h for *Staphylococcus aureus* and *Acinetobacter baylyi*. The results confirmed that complex antimicrobial coatings can be created using facile methods for silver nanoparticle synthesis and electrodeposition.

KEYWORDS: antimicrobial • lysozyme • silver • nanoparticle • electrochemistry • coating

INTRODUCTION

Infections originating from implanted devices (e.g., orthopedic fixation hardware, artificial prosthetics, endovascular stents, and catheters) are a persistent and serious health issue. The first step towards reducing these infections is inhibiting bacterial colonization on subcutaneous device surfaces. Current antimicrobial coating methods involve either modification of the physiochemical properties of the device surface or application of coatings that resist cell adhesion and biofilm formation (1). In order for coatings to be effective, they must incorporate a direct, on-contact biocide and also provide sustained antimicrobial activity, so to neutralize any initial contamination of the surface and also inhibit colonization over time from a wide range of opportunistic microorganisms. These issues and the rise of microbial resistance to commonly used antibiotics drive a continuous search for new antibiotic formulations that are amenable to adhesion and immobilization on surfaces.

One strategy given considerable attention in recent years is the use of silver on medical device surfaces and in wound dressings (2−4). These coatings are particularly attractive because silver ions act against a broad range of bacteria and yet are relatively nontoxic to mammalian cells (5, 6). While the antimicrobial effectiveness of silver coatings has been shown in the laboratory, there have been mixed results in the clinical setting (7). The past limitations of silver coatings as prophylactic treatments most likely stem from the ineffective release of silver ions from the surface and the unproductive adsorption and precipitation of silver ions in body fluids (8, 9).

More recently, silver in nanoparticle form has been shown to exhibit enhanced antimicrobial effects over previous silver formulations. The high surface-to-volume ratio of nanoparticles provides a substantial and sustained contact with the bacterial cell that is not easily quenched by other salts and proteins (10, 11). Numerous methods for silver nanoparticle synthesis and incorporation into materials are currently under investigation (12−20), and silver nanoparticle coatings are beginning to see more prevalent use in health care (1, 5, 8). In recent work, we discovered that the hydrolytic enzyme, lysozyme, catalyzes the reduction of silver, which yields a stable colloid of silver nanoparticles and active lysozyme (21). The use of lysozyme in the synthesis of silver nanoparticles is advantageous because it combines two different biocidal mechanisms into one material; lysozyme primarily inhibits growth of the Gram-type positive strains through its muramidase activity (22), while silver nanoparticles inhibit growth of both Gram-type negative and positive strains by inhibiting membrane function and enzyme activity (23). In a few cases, the synthesis of bioactive coatings has been achieved by adding noble metal nanoparticles to enzyme solutions and electrodepositing the mixture onto surfaces (24−27). Because of the unique properties of silver nanoparticles, their utility as the precur-

* Corresponding author. Tel.: 850-283-6026. Fax: 850-283-6090. Email: matt.eby.ctr@tyndall.af.mil (D.M.E.), glenn.johnson@tyndall.af.mil (G.R.J.).
Received for review March 30, 2009 and accepted June 16, 2009

† Universal Technology Corporation.

‡ Microbiology and Applied Biochemistry, Materials and Manufacturing Directorate, Air Force Research Laboratory.

DOI: 10.1021/am9002155

sor for electrodeposited coatings may produce more effective antimicrobial activities than previous methods based on conventional electrodeposition solutions (e.g., silver salt solutions). Herein, we report a method to produce antimicrobial coatings through electrophoretic deposition of silver nanoparticles formed from the lysozyme-mediated reduction of silver ions. The antimicrobial effectiveness of coated surfaces was tested against a variety of microorganisms to demonstrate the retention of antimicrobial properties within coatings.

EXPERIMENTAL SECTION

Reagents and the Synthesis of Silver Nanoparticles. Hen egg white lysozyme (~95%, ~50 000 units per mg of protein) and silver(I) acetate (99.99%) were obtained from Sigma-Aldrich (St. Louis, MO). Unless stated otherwise, all other chemicals were obtained from either Sigma-Aldrich or Fisher Scientific (Pittsburgh, PA) and were of the highest purity available. For experiments measuring the electrochemical properties of lysozyme, a lysozyme solution made from a stock powder was dialyzed against two changes of ultrapure water (1:100, v/v) using a 5000 Da molecular weight cut-off dialysis membrane (Spectra/Por cellulose ester, Spectrum Medical Industries, Houston, TX) over 24 h to remove residual buffer and salts and then stored at −20 °C in 30 mg mL^{-1} aliquots. To generate lysozyme−silver nanoparticle solutions for electrophoretic deposition, undialyzed lysozyme solutions (20 mg mL^{-1}) were made with ultrapure water and then diluted with methanol (1:1, v/v). A silver acetate solution in 50% methanol (1 mM) was then added to the lysozyme solution to produce a final concentration of 5 mg mL^{-1} lysozyme and 0.5 mM silver acetate in 50% methanol. The solution was then exposed to light for approximately 24 h to allow the formation of silver nanoparticles. The resulting lysozyme−silver colloidal suspension was stored in the dark at 4 °C to inhibit precipitation until use.

Electrochemical Measurements. Electrochemical measurements were performed in a one-compartment, three-electrode cell at room temperature using a 757 VA Computrace System potentiostat (Metrohm AG, Herisau, Switzerland). A silver rotating-disk electrode (2.0 mm disk diameter) was employed as the working electrode in conjunction with a platinum rod auxiliary electrode (15 mm × 2 mm diameter, 10 mm submerged in cell) and a Ag/AgCl electrode in saturated KCl as the reference electrode. The working electrode was stationary during measurement. Before each measurement, the working and auxiliary electrodes were cleaned by polishing with 8000 grit sandpaper and then rinsed with ultrapure water. No additional electrolyte was added to the potentiostat cell. Current−potential curves (cyclic voltammograms) were generated by linear voltage sweeps between −1 and 1 V at 0.1 V s^{-1} (vs Ag/AgCl).

Electrophoretic Deposition of Lysozyme−Silver Nanoparticles. Surfaces to accept electrophoretic deposition were stainless steel surgical blades (#10, Exelint International Co., Los Angeles, CA) and syringe needles (single-use, 22 Gauge, 1.5 in. length, Becton Dickinson Co., Franklin Lakes, NJ). Before deposition, metal surfaces were cleaned and etched, using a procedure similar to that described previously (28). Blades and needles were cleaned by ultrasonication for 15 min each in dichloromethane, acetone, and water. Clean surfaces were then etched for 1 min in a solution containing 0.25% hydrochloric acid and 2.5% nitric acid. After etching, metal surface passivation was completed in 40% nitric acid for 40 min. Blades and needles were then extensively washed with ultrapure water, dried, and stored until use.

A two-electrode electrophoretic cell was constructed that contained either a blade or a needle as the working electrode. Approximately 1 cm of the blade or needle tip was submerged into 5 mL of the lysozyme−silver nanoparticle deposition solution. A platinum wire was also submerged approximately 1 cm into the solution and served as the secondary electrode. The distance between each electrode was approximately 1 cm. A power source [1735 direct-current (dc) power supply, BK Precision, Placentia, CA] applied a dc voltage (3 V) for 10 min. After electrodeposition, blades and needles were rinsed extensively with ultrapure water and stored at room temperature.

Three additional electrophoretic coating experiments were completed to determine the individual effects that lysozyme and silver nanoparticles have on deposition and when lysozyme and silver acetate were combined in the deposition solution but without prior formation of nanoparticles. For the first two control experiments, lysozyme and silver nanoparticles were used in separate electrodeposition solutions. For electrophoretic deposition containing only lysozyme, the procedure was followed as described above, except a solution containing 5 mg mL^{-1} lysozyme in 50% methanol served as the deposition solution. For electrophoretic deposition primarily composed of silver nanoparticles, a dialysis method was used to remove soluble lysozyme from the deposition solution that was not tightly associated with nanoparticles (21). Prior to deposition, a 5 mL solution of lysozyme−silver nanoparticles was placed into a 25 000 Da molecular weight cut-off dialysis bag (Spectra/Por cellulose ester) and dialyzed against four changes of 1 L of water for 72 h to remove the majority of lysozyme. This resulted in a deposition solution that contained mostly silver nanoparticles but still contained small amounts of lysozyme. For the third control experiment, freshly mixed solutions of lysozyme (10 mg mL^{-1}) and silver acetate (1 mM) in 50% methanol (1:1, v/v) served as the electrodeposition solution and were used immediately in the electrophoretic cell in the absence of light, in order to prevent silver reduction and subsequent nanoparticle formation.

Physical and Spectroscopic Characterization. UV−visible spectroscopy was completed using a Cary 3E spectrophotometer (Varian Inc., Palo Alto, CA) and 0.5 mL quartz cuvettes. Atomic force microscopy (AFM) images were obtained using a Nanoscope V, equipped with a Multimode V scanning probe microscope and a PicoForce stage (Veeco Instruments Inc., Woodbury, NY). Blades were first dried under vacuum at 50 °C for 10 min before imaging in tapping mode, using an etched phosphorous (n)-doped silicon cantilever probe (type RTESP, Veeco Instruments Inc.). The natural frequency of the cantilever was in the 200 kHz range, and the radius of the probe tip was <10 nm. Transmission electron microscopy (TEM) was completed using a 100 CX II electron microscope from JEOL Ltd. (Tokyo, Japan). Attenuated total reflectance Fourier transform infrared (ATR FT-IR) spectroscopy was performed using a Nicolet FT-IR 6700 spectrophotometer equipped with a Smart Miracle single-bounce diamond ATR accessory (Thermo Fisher Scientific, Waltham, MA). The data collection was completed using *OMNIC 2.1* software. Before measurement, coated and uncoated blades were washed with methanol and dried at 50 °C for 30 min. For ATR FT-IR of the lysozyme stock powder, 10 μL of a lysozyme powder slurry in methanol was dried on the instrument crystal before measurement.

Measurement of the Lysozyme Activity. Qualitative measurement of the lysozyme activity in coatings was adapted from the *Micrococcus lysodeikticus* cell lysis assay in solid media, first described by Fleming (29). Blades and needles were first used to cut and puncture, respectively, solid media plates containing a suspension of 0.5 mg mL^{-1} *M. lysodeikticus* cells (Sigma-Aldrich) in a 50 mM potassium phosphate buffer (pH 8) and 1% agarose before being placed on top of the plate surface. Plates were incubated at 37 °C for 16 h and periodically inspected for cell lysis, which resulted in a clearing of the solid agar at the blade and needle contact points.

Antimicrobial Activity Assays. The following strains used in the antimicrobial assays were obtained from the American Type Culture Collection (ATCC, Manassas, VA): *Escherichia coli* (ATCC 25922), *Staphylococcus aureus* (ATCC 25923), *Klebsiella pneumoniae* (ATCC 4352), *Pseudomonas fluorescens* (ATCC 13525), *Candida albicans* (ATCC 10231), and *Staphylococcus epidermidis* (ATCC 14990). *Bacillus anthracis* Sterne strain 34F2 was obtained from Colorado Serum Co., Denver, CO (30). *Acinetobacter baylyi* strain ADP1 (31) was a gift from Dr. Ellen Neidle (University of Georgia, Athens, GA). Luria-Bertani and Yeast Mold (Difco Laboratories, Sparks, MD) were used to grow bacterial strains and *C. albicans*, respectively, in liquid and on solid media plates (plates also contained 1.5% agarose).

At the start of the antimicrobial assay, coated blades were incubated in growth media containing approximately 10^5 cells in the exponential growth phase (1 mL). Viable cells were quantitated after 0, 1.5, and 3 h of incubation by removing 100 μL from the cultures, spreading all or a serial dilution of the aliquot onto solid media, and enumerating colony-forming units (cfu). After cultures were incubated for 24 h, blades were removed from cultures and placed into fresh, sterile media (1 mL). In addition, the remaining growth media from the blade culture was diluted into fresh, sterile media (1:10 dilution). The two subcultures were incubated overnight and then visually inspected for growth. Results are the average of at least three replicates. Uncoated, etched blades were also incubated in separate cultures to ensure that cells grew in the absence of a coating material, and the etched stainless steel did not adversely affect the growth.

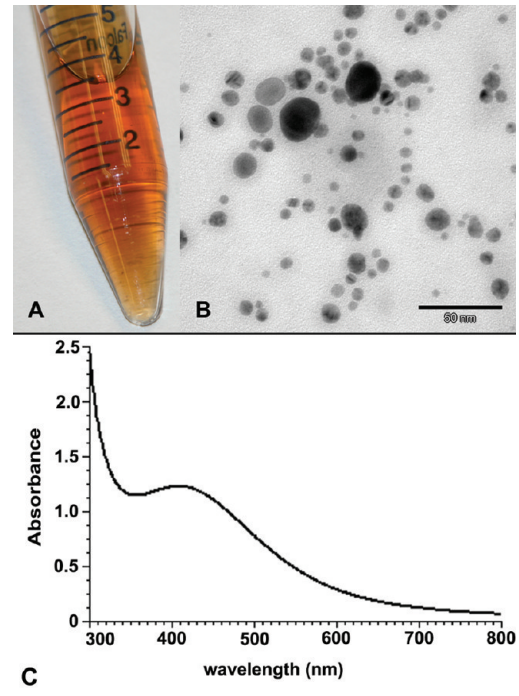

FIGURE 1. Lysozyme-catalyzed silver nanoparticles (A). TEM image of lysozyme–silver nanoparticles (B). UV–visible spectrum of lysozyme–silver nanoparticles showing a plasmon resonance absorbance maximum at 420 nm (C).

RESULTS AND DISCUSSION

Synthesis and Electrochemical Behavior of Lysozyme–Silver Nanoparticles. In our recent work, we found that stable colloids of silver nanoparticles formed from the incubation of micrograms per milliliter quantities of lysozyme and silver acetate in 100% methanol (21). The growth of silver nanoparticles was dependent upon exposure to light and only required lysozyme, which acted as the reductant and colloidal stabilizing agent. For electrophoretic deposition, the previous formulation was optimized by increasing the lysozyme concentration to 5 mg mL^{-1} and completing the nanoparticle synthesis reaction in an aqueous solution containing 50% methanol (Figure 1). The final solution contained a sufficient concentration of ionic species to facilitate electrophoretic deposition without additional electrolytes, while also maintaining a stable suspension of nanoparticles. When stored in the dark at ambient conditions, the lysozyme–silver nanoparticles can be maintained as a colloid for several months.

The electrochemical properties of lysozyme were measured using cyclic voltammetry with a silver disk electrode. Lysozyme was oxidized at 745 mV and underwent two reductions at −640 and −800 mV (Figure 2A). Repeated potentiostat cycling resulted in successively smaller peak currents, which were indicative of irreversible deposition of protein on the electrode surface (32). When silver acetate was added to lysozyme, voltammograms completed immediately after mixing show a shift in the reduction peaks of lysozyme toward a lower cathodic potential (Figure 2B). Similar voltammeric behavior has been previously reported when protein–metal complexes form in the electrochemical cell and change the electrochemical properties of the individual species (33). Considering that silver acetate alone does not produce current peaks under our conditions (dashed gray line in Figure 2B), the shift in the peak potential of lysozyme after silver addition suggests that silver associates with lysozyme and forms a new electrochemically active species. As seen with lysozyme alone, additional voltage cycles also showed that the lysozyme–silver complex was irreversibly deposited and formed a coating on the electrode surface. As silver nanoparticles developed in the lysozyme and silver acetate solution, cyclic voltammetry was completed at intermittent time intervals during incubation (0.3, 2, and 24 h). Samples were taken from the synthesis reaction for voltammeric analysis and the electrodes were polished between each use. In each case, there was no change in the potential and intensity of the current peaks, which indicated that the electrochemical properties of lysozyme were not altered during and after nanoparticle synthesis (results not shown). When silver nanoparticles were present in the potentiostat cell, a resilient red film formed on the electrode surface during repeated voltage cycling, which required removal by physical abrasion using fine-grit sandpaper. Taken together, these observations showed that lysozyme–silver nanoparticles form a complex that was electrophoretically deposited onto the electrode surface. The results led us to investigate whether the antimicrobial properties of lysozyme and silver were retained within the coatings.

Electrophoretic Deposition of Lysozyme–Silver Nanoparticles onto Stainless Steel. Stainless steel surgical blades and syringe needles were investigated as model surfaces for the coating. An electrodeposition cell was constructed using a blade or needle as the working electrode, and the tip was submerged in the lysozyme–silver

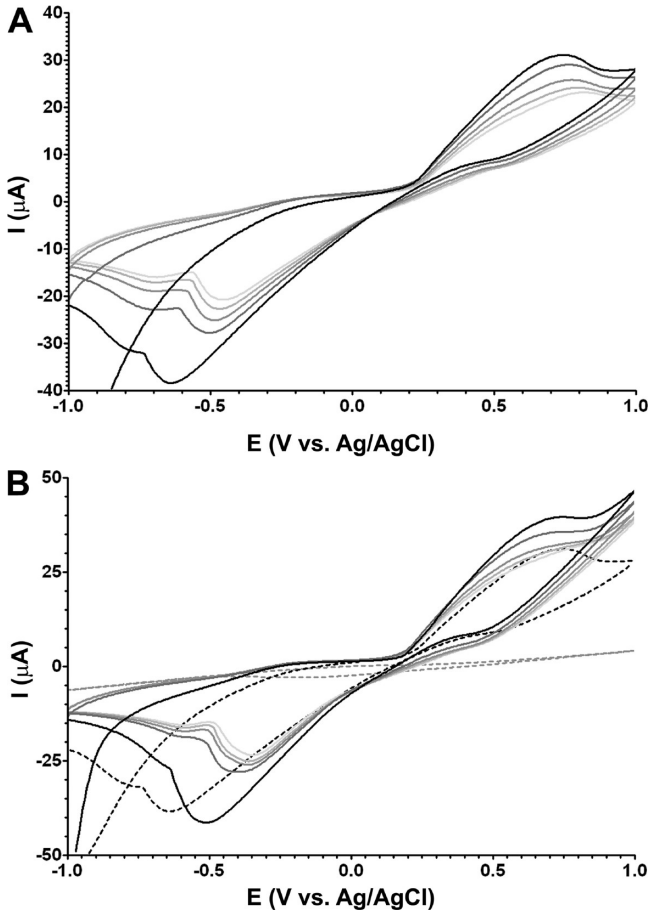

FIGURE 2. Cyclic voltammograms of pure lysozyme (A) and the lysozyme–silver nanoparticle electrophoresis solution (B) in 50% methanol. In each case, five voltammograms were recorded. The initial voltammogram is shown in black, and successive voltammograms are in increasingly lighter gray. The initial voltammogram of pure lysozyme from part A is shown as a dashed black line in part B. The voltammogram of 0.5 mM silver acetate in 50% methanol is shown as a dashed gray line.

nanoparticle solution. After a constant dc potential was applied, a red film formed on the surface of the blades and needles. Much of this coating was removed after extensive washing with deionized water, but a thin coating remained on the metal surfaces (Figure 3, left). The evenly dispersed and strongly adherent coating was not observed when any of the control solutions were used in the electrophoretic deposition assay. A uniform coating was not seen when most of the lysozyme was dialyzed from a silver nanoparticle solution prior to electrophoresis or with solutions of freshly mixed lysozyme and silver acetate, which did not contain any nanoparticles. A translucent coating was observed when only lysozyme was present in solutions, but the film was easily washed off the blade surface.

The coatings from lysozyme–silver nanoparticle electrodeposition solutions retained lysozyme, as shown by ATR FT-IR (Figure 4). The spectrum of the coated blades was identical to the spectrum of blades that were coated with lysozyme only, as well as to the spectrum of the lysozyme stock. The results confirmed that no major perturbations in the lysozyme structure occurred as a result of silver nanoparticle synthesis or electrophoretic deposition. Changes in the protein secondary and tertiary structures will alter hydrogen bonding between the CO and NH groups in the peptide backbone, which results in aberrations of the amine I, II, and III bands between 1200 and 1700 cm^{-1} (34). No such significant shifts were observed in this IR region between lysozyme-coated blades and the stock powder. In addition, coated blade surfaces were analyzed at the nanometer scale using AFM (Figure 3). A layer of spherical nanoparticles on the surface of coated blades was clearly seen in images. The AFM images of etched, uncoated blades did not have these features (results not shown). The nanoparticles visualized in the coating were similar in shape and diameter to the silver nanoparticles observed in the TEM images of the deposition solution (Figure 1). The nanoparticles were also readily seen in phase images (lighter areas, Figure 3E) and were surrounded by a material of contrasting phase (darker areas). Under closer inspection, edge enhancement illustrated in the 200 nm^2 amplitude error image (Figure 3D) showed a veinlike texture between the nanoparticles. In the corresponding phase image (Figure 3F), these features appeared in contrasting phase color to the nanoparticles. The contrast in the phase images can be used to discern between an organic material, consisting of protein or other hydrocarbon compounds, and metallic nanoparticles (35, 36). Lysozyme and crystalline silver would impart very different interactions with the AFM tip, resulting in clear differences in the phase images. Considering that the electrodeposition buffer contained primarily silver and lysozyme, the phase-contrasting materials are most likely distinct regions of these two substances. The regions surrounding the spherical protrusions on the blade surface are proposed to be areas of lysozyme packed between the silver nanoparticles. Similar grafting features have been observed in AFM phase contrast images of surfaces after the electrochemical deposition of silver nanoparticles and acrylate, where a sustained cathodic overpotential during electrodeposition forced the organic material off the silver nanoparticles and onto the electrode surface (36).

Evaluation of the Lysozyme Activity within Surface Coatings. The hydrolytic activity of lysozyme retained within electrodeposited coatings on blades and needles was investigated through an in vitro cell lysis assay designed to mimic the normal use of the instruments. Coated blades and needles were used to make incisions and punctures, respectively, into agarose infused with *M. lysodeikticus* cells. Within minutes, zones of clearing were seen at the contact site, which was indicative of cell lysis due to lysozyme hydrolytic activity (Figure 5). The spread of cell lysis over time within the agar demonstrated that the antimicrobial activity not only was retained on the surface of the blades and needles but also was transferred into the media. Blades subjected to electrodeposition using a solution containing only lysozyme demonstrated a minimal zone of clearing after incubation for 16 h, in comparison to blades coated with lysozyme–silver nanoparticles. Cell lysis was not observed with blades and needles subjected to electrophoretic deposition using solutions containing soluble silver

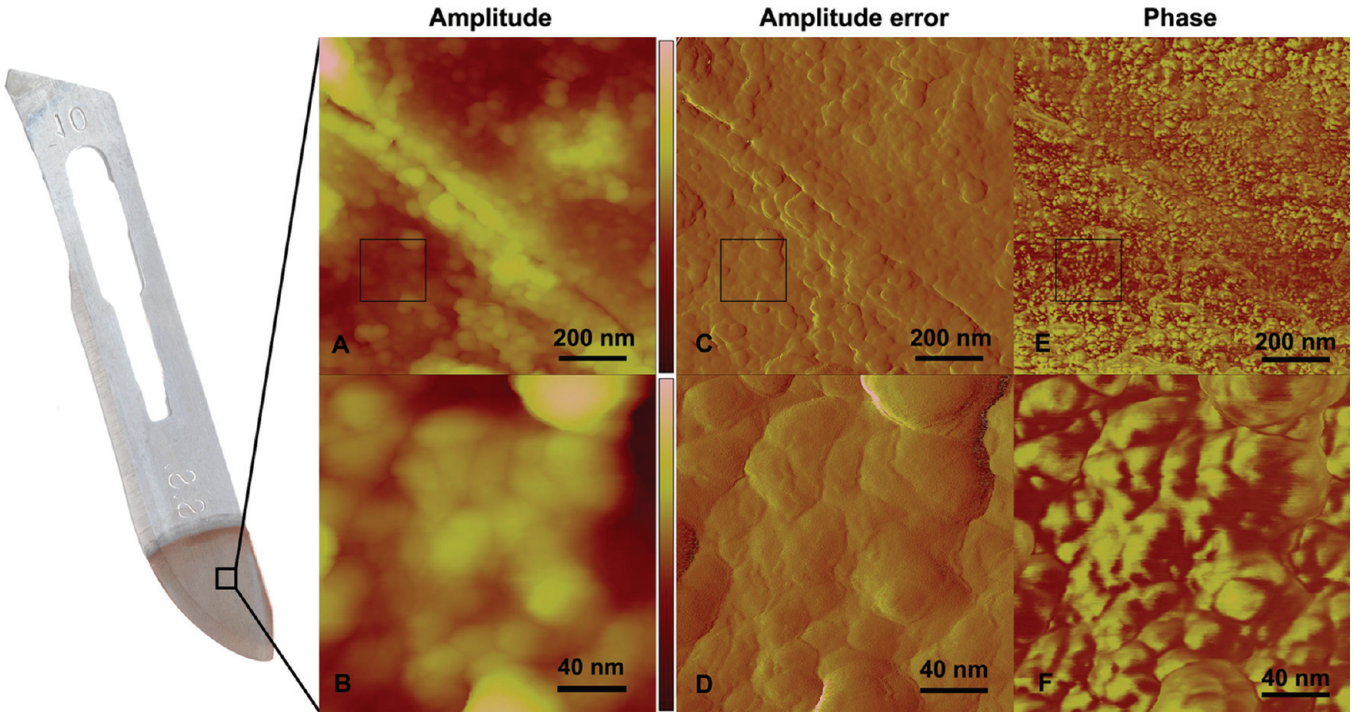

FIGURE 3. Left: Photographic image of a surgical steel blade coated with lysozyme−silver nanoparticles. Right: Typical AFM images of a coated blade. The surface area imaged was 1 μm^2 (A, C, and E) and 200 nm^2 (B, D, and F). The amplitude (A and B), amplitude error (C and D), and phase images (E and F) are shown from left to right. Height scale bars in amplitude images are 300 and 50 nm for 1 μm^2 and 200 nm^2 images, respectively. AFM of the 200 nm^2 image was completed within the boxed area of the blade surface shown in the 1 μm^2 image.

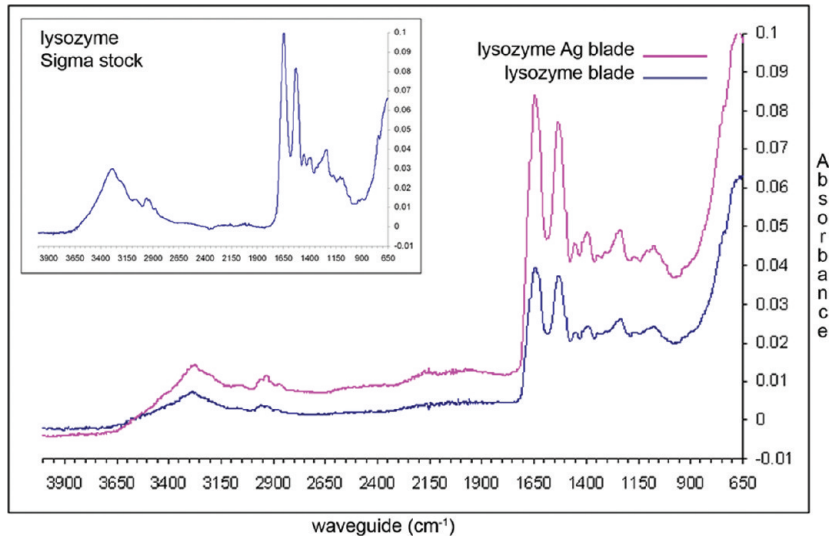

FIGURE 4. ATR FT-IR of blade surfaces after electrodeposition using either the lysozyme−silver nanoparticle solution (top spectrum) or a solution containing only lysozyme (bottom spectrum). Inset: Spectrum of the lyophilized lysozyme stock.

acetate (no nanoparticles) or only silver nanoparticles (results not shown). Considering that silver did not initiate cell lysis under these conditions, the higher activity of the lysozyme−silver nanoparticle coatings versus lysozyme alone is attributed to either a more efficient deposition of lysozyme onto the metal surface when silver nanoparticles are present or the capability of the enzyme to diffuse more rapidly from lysozyme−silver nanoparticle coatings. Either way, the unique nature of the lysozyme−silver nanoparticle coatings allowed the efficient release of active enzyme into the media, which transferred the antimicrobial properties of lysozyme throughout the cut and puncture sites.

Antimicrobial Range of Surgical Blade Coatings. The *M. lysodeikticus* lysis assay demonstrated the antimicrobial activity of the coatings. However, the contribution of silver nanoparticles to the antimicrobial activity of the coatings cannot be determined using this assay. Lysozyme is primarily bacterolytic toward Gram-type positive strains, whereas silver nanoparticles have been shown to have antimicrobial activity toward many differ-

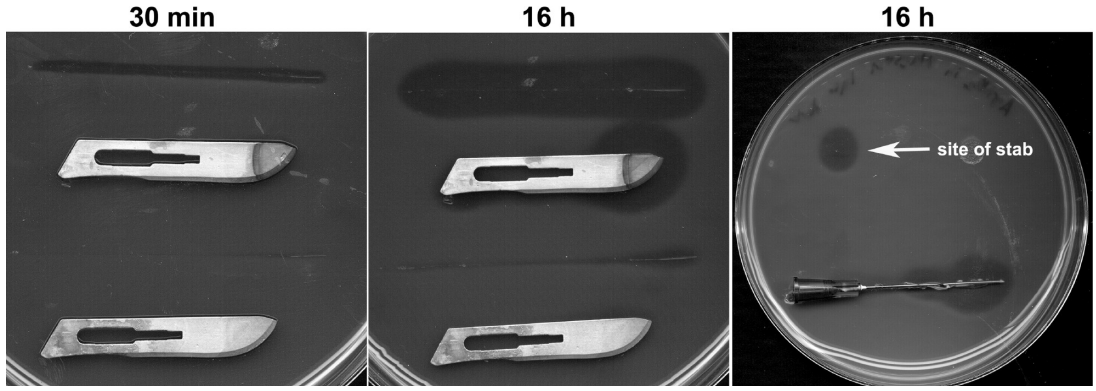

FIGURE 5. Cell lysis assay measuring the antimicrobial activity of coated blades and needles. Coated blades (left and middle) and needles (right) were used to make incisions and punctures, respectively, and then placed on top of agarose infused with *M. lysodeikticus* cells. The top blade contains a coating of lysozyme−silver nanoparticles, while the lower blade has a coating of lysozyme only. Zones of cell lysis are seen at the incision and puncture sites, as well as surrounding the blades and needles after incubation at 37 °C for 30 min and 16 h.

Table 1. Antimicrobial Activity of Coated Blades against Bacterial and Yeast Strains

	log reduction[a]		
strain	1.5 h	3 h	inhibition type[b]
Acinetobacter baylyi	2.49 ± 1.48	2.98 ± 1.75	bactericidal
Bacillus anthracis Sterne	3.50 ± 1.25	3.93 ± 0.62	bactericidal
Bacillus subtilis	4.78 ± 0.50	4.78 ± 0.50	bactericidal
Candida albicans	growth	growth	none
Escherichia coli	1.56 ± 1.38	growth	none
Klebsiella pneumoniae	3.29 ± 1.67	3.94 ± 1.14	bactericidal
Pseudomonas fluorescens	0.65 ± 0.24	0.26 ± 0.30	none
Staphylococcus aureus	2.01 ± 0.62	3.48 ± 0.53	bactericidal
Staphylococcus epidermidis	0.47 ± 0.55	0.43 ± 0.24	bacteriostatic

[a] log reduction was calculated as [log of viable cells (cfu mL^{-1}) before exposure to a coated blade] − [log of the viable cells (cfu mL^{-1}) at a time point after incubation with a coated blade]. The standard deviation is from three separate assays. [b] The inhibition type was based on log reduction values and the viability of the subcultures made from the initial 24 h incubation with coated blades. See the text for details.

ent microbial species. To determine the range of antimicrobial activity demonstrated by both components of the coating, eight different bacterial strains and one yeast strain were used in the antimicrobial assays. Coated blades were incubated with actively-growing cultures, and viable cells that remained over time were quantitated by spread-plating culture aliquots on solid media and enumerating the cfu (Table 1). Uncoated, etched blades were also incubated in separate cultures and, in each case, cells grew to high cell density, ensuring that the etched stainless steel did not adversely affect the growth (results not shown).

Demonstrating effective bactericidal activity, coated blades reduced the cell viability by >3 log within 1.5 h for *K. pneumoniae*, *B. anthracis* Sterne, and *B. subtilis* and within 3 h for *S. aureus*. A lesser biocidal effect was observed when *A. baylyi* cells were exposed to coated blades (~3 log in 3 h). Growth inhibition lasted beyond 3 h because no visible growth was observed in cultures when incubated in the presence of coated blades for 24 h. To assess if coated blades retained antimicrobial activity after exposure to cultures and also inhibited the transfer of any viable cells on blade surfaces, blades were removed from the culture, added to fresh media, and incubated for an additional 24 h. With the five sensitive strains mentioned above, there was no observed growth in the subsequent cultures. Furthermore, the culture media from the first 24 h incubation was diluted into fresh media (1:10) and incubated for 24 h to determine if any remaining viable cells could proliferate in the absence of coated blades. *S. aureus*, *K. pneumoniae*, *B. anthracis* Sterne, and *B. subtilis* did not visibly grow after the subculture. The two subsequent sets of cultures confirmed that (i) coatings were resilient and retained antimicrobial activity after an extended exposure to cells, (ii) coated blades were able to inhibit subsequent growth of any viable cells that may have attached to coated and uncoated areas of the blade during the first incubation, and (iii) coated blades demonstrated a complete kill in the initial culture after 24 h. *A. baylyi* was one exception, where one subculture grew to high cell density. We conclude that the effect on *A. baylyi* was bactericidal, but the potency of the coatings under our conditions was very close to the minimum bactericidal concentration, and growth in the one subculture was due to standard deviation or experimental error.

An initial, bactericidal effect was measured for *E. coli*, but the strain was able to recover and turbid cultures were observed after 24 h incubation. Previous work demonstrated that silver nanoparticles were an effective antimicrobial agent toward this particular strain of *E. coli* (16, 21). We did observe higher bactericidal activity when the initial number of *E. coli* cells was reduced to 10^4 in cultures (approximately 3 log reduction in viable cells within 1.5 h; data not shown). We concluded that the concentration of silver ions released

into the culture by coated blades was below the minimum inhibitory concentration for *E. coli* under the conditions of the antimicrobial assay. Similar to *E. coli*, an initial, bactericidal effect was also measured for *P. fluorescens*, but the surviving population recovered and propagated after 24 h. When *P. fluorescens* cultures were transferred and grown on solid media to enumerate viable cells, colonies originating from coated blade cultures were nearly identical with colonies grown from uncoated blade cultures but did not produce the characteristic yellow-green pyoverdine pigments that are normally observed with robust cells (37). The cause of this phenotype is not clear although it suggested that residual silver disrupted the pyoverdine synthesis and/or export from the cell.

The effect of coated blades on *S. epidermidis* was considered to be bacteriostatic. On average, culture viability did not change significantly in viability during the first 3 h after exposure to coated blades and did not grow to visible turbidity after 24 h. Upon transfer of the blades in fresh media, cultures grew to a slight turbidity, suggesting that blade coatings still inhibited *S. epidermidis* growth but had lost some of their potency. When the initial culture was subcultured into fresh media and incubated for an additional 24 h in the absence of coated blades, the cells grew normally. The subsequent cultures confirmed that the coating exerted a bacteriostatic effect on *S. epidermidis*. Under the conditions of the assays, coated blades inhibited reproduction and growth of *S. epidermidis* but did not completely kill cells. Once removed from exposure to coated blades, cells recovered and grew.

There was no apparent effect against the representative fungal strain *C. albicans*. When cultures of this yeast were exposed to coated blades, they grew at the same rate as cultures containing uncoated blades. In our previous study, the effectiveness of lysozyme−silver nanoparticle suspensions against *C. albicans* increased when lysozyme was removed from the solution (21). The results in this study were consistent with our previous findings because the coatings were created from nanoparticle suspensions that contained a considerably higher concentration of lysozyme and, as a result, were less effective against *C. albicans* cells.

CONCLUSIONS

Our studies demonstrated that composite antimicrobial coatings can be generated using methods for lysozyme-mediated silver nanoparticle synthesis and electrophoretic deposition. The coating employs two different biocidal mechanisms: the antimicrobial activity of silver ions and the muramidase activity of lysozyme. Coatings that integrate different biocidal mechanisms are of particular interest because they can minimize the selection and proliferation of resistant strains. Silver nanoparticles have already been shown to be effective in suppression of a wide range of pathogens, especially against strains resistant to mainstream antibiotics (6, 38). While the contribution of lysozyme has been shown to minimally contribute to the antimicrobial activity of the composite (21), the enzyme was essential to electrophoretic deposition and promoted the formation of homogeneous coatings on stainless steel surfaces. The nature of the coating was such that the mixture of lysozyme and silver nanoparticles facilitated strong adsorption to stainless steel surfaces, yet the active components also diffused from the coating following contact with media. The observations indicate that the physical properties of the coating are inherent to lysozyme, where the protein acts as a water-soluble adhesive and enables robust adsorption of the silver nanoparticles to the blade surface but will also permit diffusion of silver ions or release of the nanoparticles themselves once incubated in an aqueous environment. Hence, the effect could provide a persistent self-cleaning surface for the medical instruments and allow transfer of the antimicrobial activity to the contact surface during use (e.g., diffusion into the surrounding flesh following an incision, injection, or implant). With respect to implanted devices, the integration of lysozyme within the composite may also increase the biocompatibility of the coating and not hamper tissue reconstruction, compared to other silver coatings that are composed solely of inorganic material (39). Furthermore, the rapid coating method presented here employs reagents already accepted for use in the food and medical industries (40, 41), increasing its potential for transition to manufacturing for a diverse range of applications. While the coating was not effective against all strains tested in this study, further optimization of nanoparticle synthesis and deposition will improve its potency.

Acknowledgment. We thank Karen Kelly at the University of Florida Interdisciplinary Center for Biotechnology Research, Electron Microscopy Core Lab, Gainsville, FL, for generating TEM images, Robert K. Nichols for helpful discussions on electrophoretic deposition, and Kenneth Strawhecker for assistance in AFM techniques. This work was supported through funding from the Air Force Materials and Manufacturing Directorate (AFRL/RX) and the Joint Science Technology Office for Chemical and Biological Defense Project Code AA06CBT008 (Ilya Elashvili, Jennifer Becker, and Stephen Lee, Program Managers).

REFERENCES AND NOTES

(1) Hetrick, E. M.; Schoenfisch, M. H. *Chem. Soc. Rev.* **2006**, *35*, 780–789.
(2) Babu, R.; Zhang, J.; Beckman, E. J.; Virji, M.; Pasculle, W. A.; Wells, A. *Biomaterials* **2006**, *27*, 4304–4314.
(3) Hardes, J.; Ahrens, H.; Gebert, C.; Streitbuerger, A.; Buerger, H.; Erren, M.; Gunsel, A.; Wedemeyer, C.; Saxler, G.; Winkelmann, W.; Gosheger, G. *Biomaterials* **2007**, *28*, 2869–2875.
(4) Ong, S.-Y.; Wu, J.; Moochhala, S. M.; Tan, M.-H.; Lu, J. *Biomaterials* **2008**, *29*, 4323–4332.
(5) Dowsett, C. *Nurs. Stand.* **2004**, *19*, 56–60.
(6) Strohal, R.; Schelling, M.; Takacs, M.; Jurecka, W.; Gruber, U.; Offner, F. *J. Hosp. Infect.* **2005**, *60*, 226–230.
(7) Silver, S. *FEMS Microbiol. Rev.* **2003**, *27*, 341–353.
(8) Lansdown, A. B. G. *Curr. Prob. Derm.* **2006**, *33*, 17–34.
(9) Schierholz, J. M.; Lucas, L. J.; Rump, A.; Pulverer, G. *J. Hosp. Infect.* **1998**, *40*, 257–262.
(10) Baker, C.; Pradhan, A.; Pakstis, L.; Pochan, D. J.; Shah, S. I. *J. Nanosci. Nanotechnol.* **2005**, *5*, 244–249.
(11) Pal, S.; Tak, Y. K.; Song, J. M. *Appl. Environ. Microbiol.* **2007**, *73*, 1712–1720.
(12) Kim, Y. H.; Lee, D. K.; Cha, H. G.; Kim, C. W.; Kang, Y. S. *J. Phys. Chem. C* **2007**, *111*, 3629–3635.
(13) Kong, H.; Jang, J. *Langmuir* **2008**, *24*, 2051–2056.

(14) Lee, D.; Cohen, R. E.; Rubner, M. F. *Langmuir* **2005**, *21*, 9651–9659.
(15) Li, Y.; Leung, P.; Yao, L.; Song, Q. W.; Newton, E. *J. Hosp. Infect.* **2006**, *62*, 58–63.
(16) Marini, M.; Niederhausern, S. D.; Iseppi, R.; Bondi, M.; Sabia, C.; Toselli, M.; Pilati, F. *Biomacromolecules* **2007**, *8*, 1246–1254.
(17) Sambhy, V.; MacBride, M. M.; Peterson, B. R.; Sen, A. *J. Am. Chem. Soc.* **2006**, *128*, 9798–808.
(18) Vigneshwaran, N.; Kathe, A. A.; Varadarajan, P. V.; Nachane, R. P.; Balasubramanya, R. H. *Langmuir* **2007**, *23*, 7113–7117.
(19) Wang, Q.; Yu, H.; Zhong, L.; Liu, J.; Sun, J.; Shen, J. *Chem. Mater.* **2006**, *18*, 1988–1994.
(20) Zhang, Y.; Peng, H.; Huang, W.; Zhou, Y.; Zhang, X.; Yan, D. *J. Phys. Chem. C* **2008**, *112*, 2330–2336.
(21) Eby, D. M.; Schaeublin, N. M.; Farrington, K. E.; Hussain, S. M.; Johnson, G. R. *ACS Nano* **2009**, *3*, 984–994.
(22) Pellegrini, A.; Thomas, U.; von Fellenberg, R.; Wild, P. *J. Appl. Bacteriol.* **1992**, *72*, 180–187.
(23) Panáček, A.; Kvítek, L.; Prucek, R.; Kolář, M.; Večeřová, R.; Pizúrová, N.; Sharma, V. K.; Nevěčna, T.; Zbořil, R. *J. Phys. Chem. B* **2006**, *110*, 16248–16253.
(24) Lim, S. H.; Wei, J.; Lin, J.; Li, Q.; Kuayou, J. *Biosens. Bioelectron.* **2005**, *20*, 2341–2346.
(25) Luo, X. L.; Xu, J. J.; Du, Y.; Chen, H. Y. *Anal. Biochem.* **2004**, *334*, 284–289.
(26) Wu, L. Q.; Lee, K.; Wang, X.; English, D. S.; Losert, W.; Payne, G. F. *Langmuir* **2005**, *21*, 3641–3646.
(27) Zhao, G.; Xu, J. J.; Chen, H. Y. *Anal. Biochem.* **2006**, *350*, 145–150.
(28) Spoerke, E. D.; Stupp, S. I. *Biomaterials* **2005**, *26*, 5120–5129.
(29) Fleming, A. *Proc. R. Soc. London, Ser. B* **1922**, *93*, 306–317.
(30) Ireland, J. A.; Hanna, P. C. *Infect. Immun.* **2002**, *70*, 5870–5872.
(31) Juni, E.; Janik, A. *J. Bacteriol.* **1969**, *98*, 281–288.
(32) Barton, A. C.; Collyer, S. D.; Davis, F.; Gornall, D. D.; Law, K. A.; Lawrence, E. C.; Mills, D. W.; Myler, S.; Pritchard, J. A.; Thompson, M.; Higson, S. P. *Biosens. Bioelectron.* **2004**, *20*, 328–337.
(33) Pires de Castro, C. S.; Rodrigues Souza De, J.; Bloch Junior, C. *J. Inorg. Biochem.* **2003**, *94*, 365–371.
(34) Socrates, G. *Infrared and raman chracteristic group frequencies. Tables and charts*, 3rd ed.; John Wiley and Sons, Ltd.: Chichester, U.K., 2001.
(35) Lin, S.; Lee, C. K.; Lee, S. Y.; Kao, C. L.; Lin, C. W.; Wang, A. B.; Hsu, S. M.; Huang, L. S. *Cell. Microbiol.* **2005**, *7*, 1763–1770.
(36) Voccia, S.; Ignatova, M.; Jerome, R.; Jerome, C. *Langmuir* **2006**, *22*, 8607–8613.
(37) Meyer, J.-M. *Arch. Microbiol.* **2000**, *174*, 135–142.
(38) Atiyeh, B. S.; Costagliola, M.; Hayek, S. N.; Dibo, S. A. *Burns* **2007**, *33*, 139–148.
(39) Meyers, S. R.; Khoo, X.; Huang, X.; Walsh, E. B.; Grinstaff, M. W.; Kenan, D. J. *Biomaterials* **2009**, *30*, 277–286.
(40) Silver, S.; Phung, L. T.; Silver, G. *J. Ind. Microbiol. Biotechnol.* **2006**, *33*, 627–634.
(41) U.S. Food and Drug Administration, Center for Food Safety and Applied Nutrition, Office of Premarket Approval. *Agency Response Letter Generally Regarded as Safe (GRAS) Notice No. GRN 000064*; April 2, **2001**.

AM9002155